Diagnosis of Ovarian Masses with Quantitative Multi-Parametric Magnetic Resonance Imaging at 3 Tesla

A THESIS
SUBMITTED TO THE FACULTY OF THE GRADUATE SCHOOL
OF THE UNIVERSITY OF MINNESOTA
BY

Jori Susanne Carter

IN PARTIAL FULFILLMENT OF THE REQUIREMENTS
FOR THE DEGREE OF
MASTER OF SCIENCE

Levi S. Downs, Jr.

June 2012

Acknowledgements

Patrick J. Bolan, Levi S. Downs, Jr., Joseph S. Koopmeiners, Jessica E. Kuehn-Hajder, Gregory J. Metzger, and Navneeth Lakkadi significantly contributed to the implementation and authorship of this research project. This work was supported in part by grants NCRR P41 RR008079, NIBIB P41 EB015894, NIH T32 CA132715, The Randy Shaver Foundation, and the University of Minnesota Academic Health Center Faculty Seed Grant. The authors wish to thank Diane Hutter R.N. for managing and preparing the patients, and to Siemens for provide works-in-progress software packages.

Abstract

Purpose: To identify quantitative MRI parameters which are associated with ovarian malignancy.

Materials and Methods: Women scheduled for surgical removal of a suspected ovarian mass underwent preoperative imaging of the pelvis with 3 Tesla MRI. Dynamic contrast-enhanced (DCE) MRI with pharmacokinetic modeling, quantitative T_2 mapping, and diffusion weighted imaging with quantitative mapping of the water diffusion parameters were performed. Regions of interest (ROIs) were drawn by a blinded radiologist and categorized as predominantly cystic or solid. Masses were histologically categorized as benign or malignant after surgery. Mean ROI values for all quantitative imaging parameters were compared between benign and malignant masses using generalized estimating equations. In addition, we compared the classification accuracy using a combination of histogram characteristics from T_2 map ROIs to the classification accuracy for the ROI mean alone.

Results: 34 women were included in the study (12 malignant, 22 benign). We observed significant differences in several DCE-MRI parameters between solid benign masses and solid malignant masses. Toft's rate constant (k_{ep}) was most significant, with malignant masses being significantly higher than benign masses. Quantitative T_2 values ($p=0.003$) and signal intensity on T_2 weighted imaging ($p=0.008$) were also significantly higher in solid ROIs of malignant masses. A linear combination of the mean, standard deviation, skewness and kurtosis of T_2 within solid regions provided better classification accuracy than the mean of T_2 alone.

Conclusion: Quantitative parameters from DCE-MRI and T_2 mapping can independently differentiate benign from malignant ovarian masses.

Table of Contents

List of Tables

List of Figures

Introduction

Ovarian cancer is the leading cause of death from gynecologic cancers among women in the United States (1). Five-year survival rates decrease dramatically from 90% in stage I to 30-40% in stage III and IV patients (2). The near absence of symptoms in early stage and the lack of effective screening tools both contribute to the poor overall survival. Improved imaging techniques can improve the management of patients with adnexal masses. More accurate diagnostic imaging can identify patients for referral to gynecologic oncologists in cases at high risk for malignancy, which has been shown to improve survival rates compared to surgical care given by general gynecologists or general surgeons (3,4). Better imaging may also improve assessment of treatment response, and with sufficient development and validation, could be used for screening in high-risk populations.

Several diagnostic modalities, including ultrasonography (US), computed tomography (CT), and MRI have been investigated as potential diagnostic and screening tools, but none to date have demonstrated sufficient accuracy to predict malignancy either alone or as a part of screening strategy (5-15). Conventional contrast-enhanced MRI has an 84%-93% accuracy to differentiate between malignant and benign lesions (13-15). The interpretation of these images, however, is subjective and may vary depending on the experience of the reader (14). There are a number of objective physical parameters that can be measured with MRI, including relaxation rates, permeability and perfusion parameters derived from dynamic contrast enhanced (DCE) MRI, and diffusion-related parameters. Independently, several of these parameters have been found to be associated

with ovarian malignancy: malignant masses have been shown to have shorter T_2 values (16), increased perfusion based on DCE-MRI parameters (17,18), and shorter water apparent diffusion coefficients (ADC) (19,20) than benign masses.

The goal of this study was to assess the feasibility of making multiple quantitative parametric measurements within a single study, and to identify which parameters can discriminate between benign and malignant masses. Additionally, we sought to determine whether parameter heterogeneity within a region of interest (ROI), represented by a combination of histogram characteristics, could provide additional information for classifying masses as benign or malignant beyond the mean parameter value. We therefore developed a quantitative multi-parametric MRI protocol, applied it in a pilot study of patients with ovarian masses, and compared our findings to surgical pathology.

Materials and Methods

Patient Characteristics

Approval for this study was obtained from our Institutional Review Board (IRB). Thirty-seven subjects who were scheduled for surgical removal of a suspected ovarian mass (based on conventional MRI, CT, or US imaging) and had no contraindications for MRI were enrolled and gave written consent. Subjects with a contraindication to receive gadolinium-DTPA or who had a glomerular filtration rate < 60 mL/min/1.73 m^2 were allowed to participate in the study without the administration of contrast or performance of DCE-MRI. All subjects were evaluated with quantitative MR scanning prior to surgical resection with histological verification.

MRI scans were performed using a 3 Tesla MR scanner (TIM Trio, Siemens, Erlangen, Germany). The images were acquired with patients in the supine position and fitted with standard body matrix and spine array receive coils. Glucagon (0.5 mg intravenous) was given twice, once before scanning and again just prior to the DCE-MRI sequences to minimize small bowel motility in 12 patients (IRB approval of glucagon occurred mid-study). After localizer scans, anatomical imaging was performed using conventional multi-slice T_2-weighted fast spin-echo images in the axial plane (parameters for all sequences provided in Table 1), and also the coronal and sagittal planes, followed by 3-dimensional T_1-weighted fat-suppressed axial images covering the pelvis from the pubic symphysis to the sacral promontory. The anatomical images were then used to identify a target region. Three quantitative imaging series (detailed below) were then acquired in the axial plane over the target region: T_2 mapping, ADC mapping, and DCE imaging.

Quantitative Imaging

Reconstructions for all three quantitative methods were performed offline using Matlab (Mathworks, Natick, MA) to produce parameter maps in DICOM format for subsequent analyses. The T_2 mapping acquisition used a two-dimensional multi-echo spin-echo sequence (parameters in Table 1). The multi-echo image set was thresholded to eliminate noise pixels and then fit pixel-by-pixel to a monoexponential decay function to create a T_2 parameter map.

Diffusion weighted images (DWI) were acquired using a single-shot fat suppressed echo-planar imaging sequence with three b-values (b=0, 100, 800 s/mm^2),

three orthogonal diffusion traces, and four averages. All three b-value images were noise-masked, log-transformed, and then fit pixel-by-pixel with a linear model to produce parametric maps of the water ADC. Additional diffusion parameters were calculated using the theory of intravoxel incoherent motion (IVIM) proposed by Le Bihan et al. (21), which aims to separate true diffusion from perfusion effects. Following this method, the b=100 s/mm^2 and 800 s/mm^2 images were used to calculate maps of the true diffusion coefficient IVIM-D, and subsequently the perfusion fraction IVIM-F_p.

DCE acquisitions consisted of a series of forty 3D fat-suppressed gradient echo volumes, with a temporal resolution of 8.45 s/frame. Intravenous contrast injection (0.1 mmol/kg, 3 mL/s, 20 mL saline flush) was started after completion of four complete frames. The dynamic time series was noise masked and analyzed pixel-by-pixel using three previously established techniques. First, the normalized signal intensity was fit to a sigmoid function, as previously shown in ovarian cancer by Thomassin-Naggara et al. (18), to estimate the enhancement amplitude (EA), time of half rising T_h, and maximal slope (MS) of the sigmoid curve. Secondly, the signal intensity was converted to a concentration by assuming a fixed pre-contrast T_1 value of 1500 ms, as suggested by Guo et al. (22). The first 60 seconds after contrast injection were integrated to calculate the initial area under the Gadolinium concentration curve (IAUC60). Finally, assuming a fixed, population averaged arterial input function (23), the Gd concentration curve was fit to the extended Tofts' two-compartment model (24) to estimate the transfer constant K_{trans}, the rate constant k_{ep}, and the relative volume of the extravascular extracellular space, v_e.

In addition to these eleven quantitative parameters, normalized values for IAUC60, EA, and the axial T_2-weighted anatomical image were produced by dividing by the mean value of an ROI placed adjacent skeletal muscle (piriformis when possible, gluteus maximus otherwise) to normalize for variation in cardiac output and system calibrations between subjects. The quantitative parameters assessed are summarized in Table 2.

Analysis

A blinded radiologist (6 years of experience in pelvic MRI) was presented with the anatomical images on an Osirix workstation (25) and asked to prescribe two-dimensional polygonal ROIs on a representative slice for each distinct region larger than 2 cm within the ovarian mass. Each ROI was then identified as predominantly cystic or solid based on the T_2-weighted anatomical images. ROIs were copied to the parametric maps, with minor manual adjustments as needed to adjust for motion between the acquisitions and distortion on the DWI images. Histograms were generated for each ROI on all intersecting parametric maps and summary statistics (mean, standard deviation, skewness, and kurtosis) were recorded. Noise-masked pixels were excluded from the analysis.

The primary analysis compared the mean value of each parameter in each ROI by histology outcome using generalized estimating equations with exchangeable working correlation structure to account for the potential correlation between multiple ROIs from the same subject (26). Secondary analyses were performed by considering the solid and cystic ROIs separately. Bonferroni corrections for multiple comparisons were not applied

in these exploratory analyses. For the histogram analysis, we compared the classification accuracy of the ROI mean value alone versus a linear combination of histogram characteristics (mean, standard deviation, skewness, and kurtosis) from each ROI. We developed a predictive model for histology outcome with these four values using logistic regression. The classification accuracy of our model was evaluated using the receiver-operating characteristic (ROC) curve, which was estimated using leave-one-out cross validation (CV) to correct for overfitting (27). We used the area under the ROC curve (AUC) to compare the classification accuracy our fitted model to the classification accuracy for the mean ROI value alone. Confidence intervals for the AUC were estimated by bootstrap (28). All statistical calculations were performed with the R statistical software environment (29) and used a 0.05 significance level.

Results

A total of 37 women with adnexal masses gave informed consent and were enrolled in the study. All subjects were scheduled for surgical removal of at least one ovary. One subject was excluded from the analysis because her mass was not ovarian, and two were excluded because they had low malignant potential/borderline ovarian tumors. Thirty-four women were included in the analysis, 12 with malignant ovarian masses and 22 benign. Mean age was 53.6 years (range 34–87). The histologic diagnoses of the 37 women enrolled are detailed in Table 3. Several of these subjects did not have the full set of parametric data included in the analyses: ten subjects were unable to receive gadolinium-DTPA due to contraindications and therefore had no contrast-related

parametric maps; three subjects had diffusion-weighted imaging that was judged unacceptable due to artifacts and therefore had no diffusion-related parametric maps. All 34 subjects had acceptable T_2-weighted imaging and T_2 maps. The full anatomic and quantitative imaging protocol was completed in an average of 52 minutes (range 42-64).

Using the anatomical images, the radiologist prescribed a total of 109 lesion ROIs in the 34 subjects. Cystic ROIs were more common: the 22 benign cases included 8 solid ROIs and 41 cystic ROIs, whereas the 12 malignant cases included 20 solid and 40 cystic ROIs. The ROIs were then transferred to all overlapping parametric maps for each of the 15 parameters in Table 2. Note that the parametric acquisitions had reduced coverage in the slice direction compared to the anatomical images, and therefore not all ROIs were representable in all parametric maps. A total of 1696 combinations of ROI and parametric map were considered for subsequent analyses. Examples of ROIs on anatomical and parametric images are given for a benign case (Figure 1) and a malignant case (Figure 2).

The first analysis assessed the mean parametric value within each ROI to identify which MRI parameters were associated with malignancy. Both solid and cystic ROIs were included in this analysis. The results are summarized in Table 4. Most of the DCE parameters had significantly higher mean values in malignant masses compared to benign masses, including IAUC, IAUC-ref, K_{trans}, k_{ep}, sigmoid EA, and sigmoid EA-ref ($p<0.001$ in all cases). Additionally, the mean values from the T_2 maps were significantly lower in malignant masses compared in benign masses ($p=0.028$). There were no statistically significant differences with the diffusion-related parameters.

To correct for the potentially confounding effect of cystic versus solid ROIs, the analysis was repeated separately for solid ROIs and cystic ROIs. The results from analyzing only the solid ROIs are summarized in Table 5. Several DCE parameters were significantly different between benign and malignant solid regions, including IAUC-ref, k_{ep}, sigmoid EA-ref, and sigmoid T_h ($p=0.028$, <0.001, 0.025, 0.019, respectively). With the cyst ROIs removed, the T_2 values are higher in malignant solid regions, with significant differences in the T_2 map, the T_2 weighted image signal intensity (T_2-w) and the normalized signal intensity (T_2w-ref) ($p=0.003$, 0.008, <0.001, respectively). No difference was found in ADC or D, but the perfusion fraction F_p was significantly lower in malignant solid regions ($p=0.043$).

Analyzing the predominantly cystic ROIs, it was found that several DCE parameters had higher mean values in malignant cystic regions compared to benign cystic regions, including IAUC ($p<0.001$), IAUC-ref ($p=0.013$), K_{trans} ($p=0.001$), sigmoid EA ($p=0.002$), and sigmoid EA-ref ($p=0.001$) (data not shown). No significant differences were found with the T_2 parameters or the diffusion-related parameters.

Finally, we compared the classification accuracy of the ROI mean value alone versus a linear combination of histogram characteristics from each ROI. For this analysis, the data were filtered to select only those ROI/parameter map combinations with reliable distribution metrics: ROI/parameter map combinations that had fewer than 100 pixels after noise thresholding, or less than 33% pixels included after noise thresholding were removed from the analysis. After this filtering, the remaining data contained too few ROIs to adequately assess the DWI and DCE parameters, so the histogram analysis

focused solely on the T_2-related parameters. Figure 3 gives examples of ROIs on T_2 maps and their associated histogram characteristics for benign and malignant cases.

Table 6 presents AUC for the mean T_2 imaging parameters and for a linear combination of the mean, standard deviation, skewness and kurtosis for each T_2 imaging parameter. The CV adjusted AUC for a linear combination of the four histogram characteristics for T_2 map increased to 0.90 (95% CI: 0.83, 1.00), compared to an AUC of 0.81 (0.56, 1.00) for the mean alone. This suggests there is additional information for predicting histology outcome beyond the mean of the T_2 map. In contrast, the AUC for T_2w and T_2w-ref actually decreased when adding additional histogram characteristics to the model, suggesting that the additional data are simply adding noise to the model and are not useful for predicting outcome.

Discussion

In this work we have demonstrated the feasibility of performing multiparametric, quantitative MRI for the characterization of ovarian masses, and found several parameters based on DCE-MRI, diffusion imaging, and T_2 relaxometry that were significantly associated with malignancy. The most objective findings were based on the first analysis, which used only ROI means and included all ROIs without subjectively distinguishing between predominantly cystic and solid ROIs. For this analysis, both DCE-MRI and T_2-based acquisitions produced significant parameters, while diffusion imaging did not. These findings, however, were confounded by composition of the ROIs: predominantly cystic regions generally have longer T_2 values and do not enhance, and purely cystic masses are more likely to be benign.

The second analysis, which used only ROI means and only in predominantly solid ROIs, is more relevant to the diagnostic setting where the radiologist is concerned about suspicious solid regions. In this analysis, several parametrics from DCE-MRI, T_2 imaging, and diffusion imaging were associated with malignancy. The DCE-MRI findings were expected and consistent with previous literature (18), as malignant ovarian masses are known to have increased vascularity. Significant associations were found in parameters derived from each of the three distinct DCE-MRI analysis approaches (area under curve, sigmoid fitting, and pharmacokinetic modeling), suggesting that the diagnostic information is inherent in the data and robust with respect to analysis method. Our finding that quantitative T_2 mapping was associated with ovarian malignancy has not been previously reported. This is, however, consistent with the practice of using hypo- and hyper-intensity on T_2-weighted imaging as a diagnostic feature (16), but with the added advantage of being assessed quantitatively. The diffusion parameters performed more poorly than expected, with no association between ADC in either the solid-only or the solid+cyst analysis. This finding was inconsistent with previous reports using 1.5T MRI (19,20,30-33). This may be attributable to our sequence optimization; we scanned with a high resolution (192x192 matrix) while using a large acceleration factor (R=3) to keep the echo train short, and this approach may have led to insufficient signal-to-noise ratio (SNR). Further work is warranted to optimize the diffusion-weighted imaging methods for high-resolution and good SNR at 3T. We did find that the perfusion fraction F_p, as estimated by the IVIM technique, was lower in malignant solid regions than in benign solid regions. This finding should be interpreted cautiously, as it is inconsistent

with the increased vascularity shown in our DCE-MRI findings. The 3 b-value technique we used to calculate F_p was consistent with the originally reported IVIM method (21), but the F_p maps had generally low signal-to-noise, and more b-values should be used in future studies to assess IVIM parameters.

The histogram analysis illustrates that other characteristics of the T_2 map distribution beyond the mean provide additional information for discriminating between benign and malignant regions. One explanation may be that malignant solid masses have small necrotic regions (14), whereas the benign solids generally appeared to be more fibrous and uniform. Considering all three analyses, the quantitative T_2 mapping was stronger than T_2-weighted imaging signal intensity, with or without normalization by a reference ROI. This T_2 mapping has the advantage of removing receive coil sensitivity, T_1 weighting, and proton density effects, and is therefore are more direct reflection of the underlying tissue relaxation rate.

Our study has several limitations. First, for the number of parameters investigated and the multiple comparisons performed, the number of subjects enrolled was small. This may decrease the strength of the associations that were seen in this exploratory study. Second, we did not compare the performance of the metrics with conventional interpretation of the anatomic images, as the study was designed to identify potential diagnostic biomarkers rather than assess diagnostic performance. Third, due to variations in spatial coverage between the imaging methods as well as the small study size, we did not have sufficient data to assess the feasibility of using combined parameters (e.g., T_2 and ADC together) in a diagnostic model. Fourth, borderline ovarian tumors comprised

5.4% of patients with ovarian masses who were enrolled in our study (n=2), and they were excluded from the analysis because of the small number. The inclusion of larger numbers of borderline tumors in future trials could be important because there may be distinct differences between the quantitative MRI values in borderline ROIs compared to benign and malignant ROIs. Borderline ovarian tumors are treated surgically, so it would be valuable to differentiate them from benign masses.

Practical Applications

The development of MRI techniques for improved diagnostic technology and potential screening and treatment monitoring applications motivates our investigation into quantitative MRI. The possibility of developing a non-contrast ovarian MRI exam, using quantitative T_2 mapping along with conventional image interpretation, would reduce scan times and cost and could potentially be used for screening patients with high-risk for developing ovarian cancer. Additionally, T_2 mapping methods may be used to increase the accuracy of a contrast-enhanced MRI study for the characterization ovarian masses.

Tables and Figures

Table 1. Parameters of MR sequences

	T_2-weighted axial	T_2-weighted coronal & sagittal	T_1-weighted axial	T_2 map	DWI	DCE
TR (ms)	3350	7380	4.0	3000	4000	3.5
TE (ms)	95	104	1.4	13-324 in 24 steps	53	1.2
Echo-train length	29	29	-	24	64	-
Flip angle (°)	90/120	90/120	10	90/180	90/180	8
Section thickness (mm)	4.0	4.0	3.0	3.0	4.0	4.0
# Sections	36	30	52	7	24	22
Readout Field of view (mm)	280-420	280-420	250-400	240-380	300-400	240-320
Phase encode Field (% of readout)	75%	75%	75%	75%	100%	100%
Matrix	384x384	320x240	384x384	384x258	192x192	192x164
Parallel Reduction Factor	2	-	-	-	3	-
Acquisition time (s)	117	120	41	296	132	8.45

Table 2. Description of the multiple MRI parameters.

Category	Parameter	Description	Units
DWI	ADC	Apparent diffusion coefficient	mm^2/s
	IVIM-D	IVIM-derived diffusion coefficient	mm^2/s
	IVIM-fp	IVIM-derived perfusion fraction	(ratio)
DCE	IAUC60	Initial area under the Gd concentration curve, 60 seconds	mM*s
	IAUC60-ref	IAUC60 normalized by muscle reference	(ratio)
DCE Tofts	Ktrans	Tofts' volume transfer constant	min^{-1}
	k_{ep}	Tofts' rate constant	min^{-1}
	ve	Tofts' relative volume of EES per unit volume of tissue	(ratio)
DCE sigmoid	EA	Sigmoid enhancement amplitude	a.u.
	EA-ref	Sigmoid EA normalized by muscle reference	(ratio)
	Th	Sigmoid time of half-rising	S
	MS	Sigmoid maximum slope	a.u.
T_2	T_2w	Axial T2w anatomical image signal intensity	a.u.
	T_2w-ref	Axial T2w anatomical image signal intensity normalized by muscle reference	(ratio)
	T_2	Transverse relaxation time constant	Ms

Table 3. Characteristics and histology of all women enrolled.

Patient No.	Age	CA125	Largest dimension of mass, encompassing all ROIs (cm)	# Cystic ROIs	# Solid ROIs	Diagnosis	Histologic subtype
1	41	187	9	1	1	Benign	Endometriosis
2	62	194	27.3	1	1	Malignant, stage IA	Clear cell carcinoma
3	41		7.9	5	0	Benign	Endometriosis
4	43	72	11.6	3	0	Benign	Mucinous cystadenoma
5	63	9	4.3	0	2	Benign	Fibroma
6	37	96	14.1	4	0	Benign	Adenofibroma and endometriosis
7	54	16	24.3	3	0	Benign	Hemorrhagic cyst
8	62	5	5.9	0	1	Benign	Brenner tumor
9	39		4.5	1	0	Benign	Endometriosis
10	50	2267	10.9	0	1	Malignant, stage II	Fibrosarcoma
11	49	8	5.1	1	0	Benign	Adenofibroma
12	58	15	20.9	1	0	Benign	Mucinous cystadenoma and endometriosis
13	39	24	18.6	1	0	Benign	Mature teratoma
14	52	11	18.8	3	1	Benign	Serous cystadenoma
15*	44	7	6.6	3	0	Borderline, Stage IA	Serous cystadenoma
16	68	142	9.7	5	2	Malignant, stage IIIC	Serous adenocarcinoma
17	75	41	18.7	4	0	Malignant, stage IA	Mucinous adenocarcinoma
18	51	1374	11.3	5	1	Malignant, stage IV	Serous adenocarcinoma
19	59	7	4.1	1	0	Benign	Normal
20	67	7	3.2	0	1	Benign	Serous cystadenoma
21	75	249	9.1	2	1	Malignant, stage IIIC	Serous adenocarcinoma
22	69	125	10.3	1	3	Malignant,	Serous

						stage IIIC	adenocarcinoma
23	45	22	20.5	4	0	Benign	Mucinous cystadenoma
24	46	795	16	3	3	Malignant, stage IA	Endometrioid adenocarcinoma
25	49	9779	24.4	5	3	Malignant, stage IIIC	Serous adenocarcinoma
26	35	13	3.8	2	1	Benign	Serous cystadenoma
27	87	5810	16.7	3	1	Malignant, stage IIIC	Serous adenocarcinoma
28	52	18	9.1	1	0	Benign	Serous cystadenoma
29*	74	52	10.1	2	2	Borderline, stage IC	Endometrioid adenocarcinoma
30*	48	16	10.4	2	1	Borderline	Uterine smooth muscle tumor of undetermined malignancy
31	45	21	17.3	5	0	Benign	Mucinous cystadenoma
32	46	482	28.2	6	2	Malignant, stage IIC	Serous adenocarcinoma
33	49	845	14.3	5	2	Malignant, stage IV	Serous adenocarcinoma
34	34	86	4.3	2	0	Benign	Hemorrhagic cyst
35	64	13	4.3	0	1	Benign	Fibrothecoma
36	70	24	2.9	1	0	Benign	Epithelial inclusion cyst of the ovary
37	49	61	8.7	2	0	Benign	Serous cystadenoma

*Subjects 15, 30, and 29 were excluded from the study for non-ovarian pathology or borderline tumors.

Figure 1. Example of multiparametric images for a benign serous cystadenoma (subject #37). (a) Anatomical T_2-weighted image with ROI on the large cyst. (b) T_2 map (ms), (c) ADC map (10^{-6} mm^2/s), and (d) Toft's model k_{ep} map (min^{-1}) overlaid on the anatomical image with ROI indicated. The quantitative maps indicate the cystic fluid has a long T_2 (mean 1877 ms), high ADC (mean 2.7 x 10^{-3} mm^2/s), and no contrast enhancement. Also visible is a hemorrhagic corpus luteum (white arrow), whose ROI was drawn on an adjacent slice, that exhibits short T_2, negligible enhancement, and low SNR on the diffusion images.

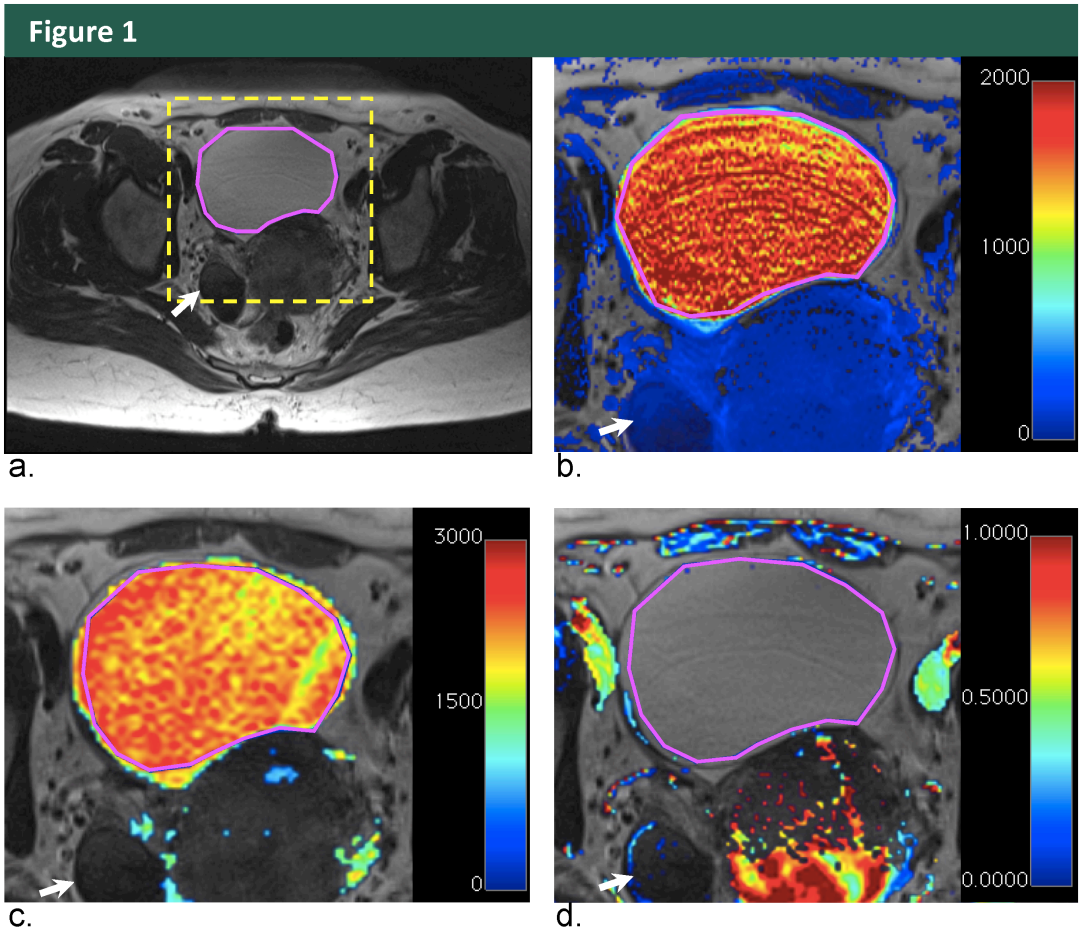

Figure 2. Example of multiparametric images for a stage IIIC serous adenocarcinoma of the ovary (subject #21). (a) Anatomical T_2-weighted image with ROI on the largest solid component of the mass. (b) T_2 map (ms), (c) ADC map (10^{-6} mm^2/s), and (d) Toft's model k_{ep} map (min^{-1}) overlaid on the anatomical image with ROI indicated. The maps show this solid region has a relatively short T_2 (118.5 ms) and low ADC (mean 0.86 x 10^{-3} mm^2/s), suggestive of high cellularity. The high k_{ep} value (mean 0.45 min^{-1}) indicates the mass is mostly well-vascularized with regions of poor perfusion. Cystic regions of the same complex mass (white arrows) exhibit variable T_2 values, high ADC, and low enhancement.

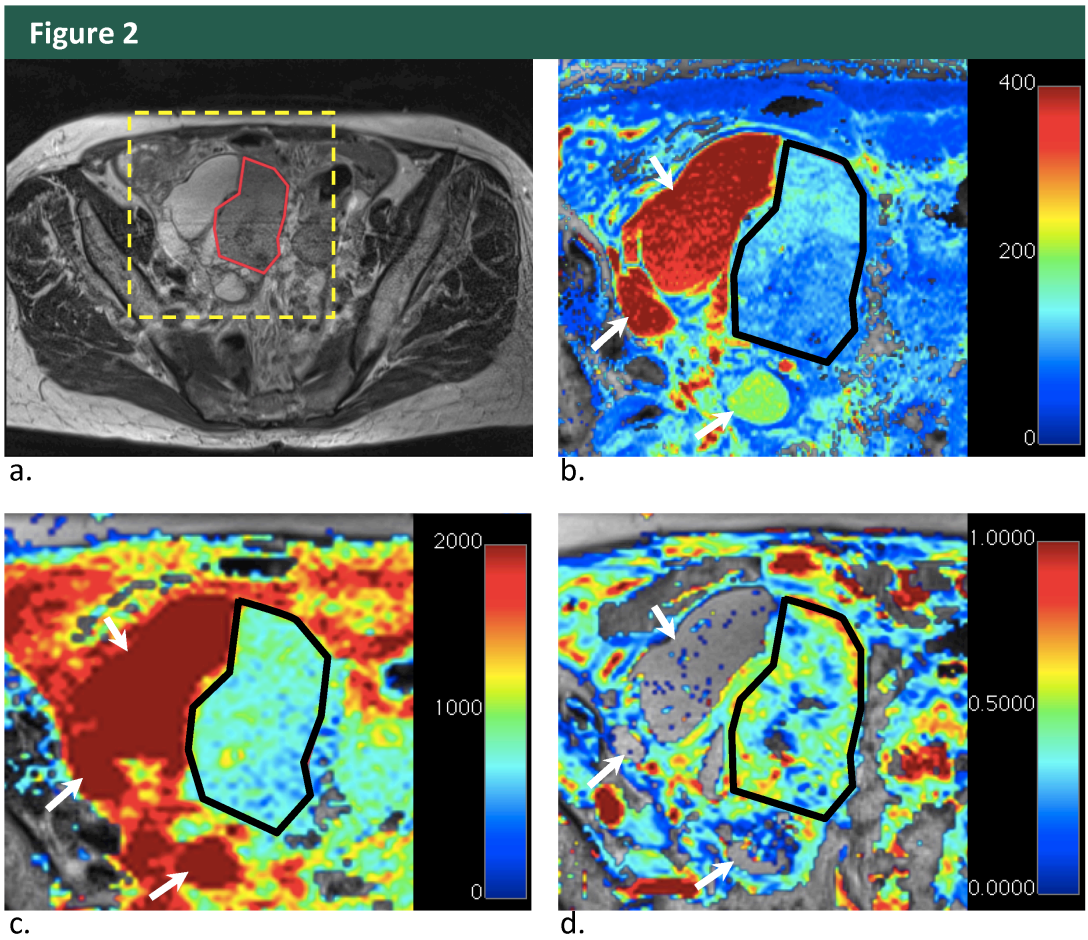

Table 4. The mean values in solid and cystic ROIs combined.

Parameter	Benign			Malignant			p-value
	N subject	N ROI	Mean value	N subject	N ROI	Mean value	
DWI							
ADC (mm^2/s)	20	40	1924.88	11	50	1747.79	0.162
D (mm^2/s)	19	37	1872.46	11	50	1700.96	0.224
F_p	19	37	8.35	11	50	9.01	0.741
DCE							
IAUC (mM*s)	14	27	0.90	9	40	3.35	<0.001 *
IAUC-ref	13	26	1.04	9	40	3.69	<0.001 *
K_{trans} (min^{-1})	15	33	0.01	9	40	0.05	<0.001 *
k_{ep} (min^{-1})	15	33	0.23	9	40	0.40	<0.001 *
v_e	15	33	0.28	9	40	0.27	0.805
sigmoidEA (a.u)	14	27	0.21	9	40	0.54	<0.001 *
sigmoidEA-ref	13	27	0.80	9	40	2.39	<0.001 *
sigmoidTh (s)	15	33	25.75	9	40	28.29	0.432
sigmoidMSx10^3 (a.u.)	15	33	142.64	9	40	107.91	0.199
T_2							
T_2 w (a.u.)	22	48	951.45	12	59	844.45	0.211
T_2 w-ref	22	48	4.11	12	59	3.44	0.080
T_2 map (s)	22	47	452.85	11	43	271.38	0.028 *

* Denotes significance at the p=0.05 level

Table 5. The mean values of solid ROIs in benign and malignant ovarian tumors.

Parameter	Benign			Malignant			p-value
	N subject	N ROI	Mean value	N subject	N ROI	Mean Value	
DWI							
ADC (mm^2/s)	6	6	1249.35	10	16	1143.44	0.609
D (mm^2/s)	6	6	1187.09	10	16	1094.90	0.668
F_p	6	6	11.27	10	16	8.95	0.043 *
DCE							
IAUC (mM*s)	4	4	3.79	9	16	6.89	0.066
IAUC-ref	4	4	3.67	9	16	7.47	0.028 *
K_{trans} (min^{-1})	4	4	0.06	9	16	0.10	0.069
k_{ep} (min^{-1})	4	4	0.27	9	16	0.47	<0.001 *
v_e	4	4	0.30	9	16	0.26	0.370
sigmoidEA (a.u)	4	4	0.69	9	16	0.89	0.239
sigmoidEA-ref	4	4	2.43	9	16	3.83	0.025 *
sigmoidTh (s)	4	4	38.06	9	16	26.18	0.019 *
sigmoidMSx10^3 (a.u.)	4	4	48.83	9	16	91.31	0.129
T_2							
T_2 w (a.u.)	7	8	426.61	11	19	621.33	0.008 *
T_2 w-ref	7	8	1.704	11	19	2.58	<0.001 *
T_2 map (s)	7	8	81.92	10	18	128.90	0.003 *

* Denotes significance at the p=0.05 level

Figure 3. Illustration of the distribution of T_2 values within solid ROIs. Top row shows the (a) T_2 map with ROI in a solid region of a benign fibrothecoma (subject #35), and (b) histogram of T_2 values from the ROI. Bottom row shows a (c) T_2 map and ROI in a solid region of a malignant serous adenocarcinoma (subject #33) and (d) associated histogram. In this comparison the benign solid ROI had a shorter mean T_2 value and a more uniform distribution of T_2 values (b) compared to the longer T_2 values and more skewed distribution for the malignant solid ROI (d).

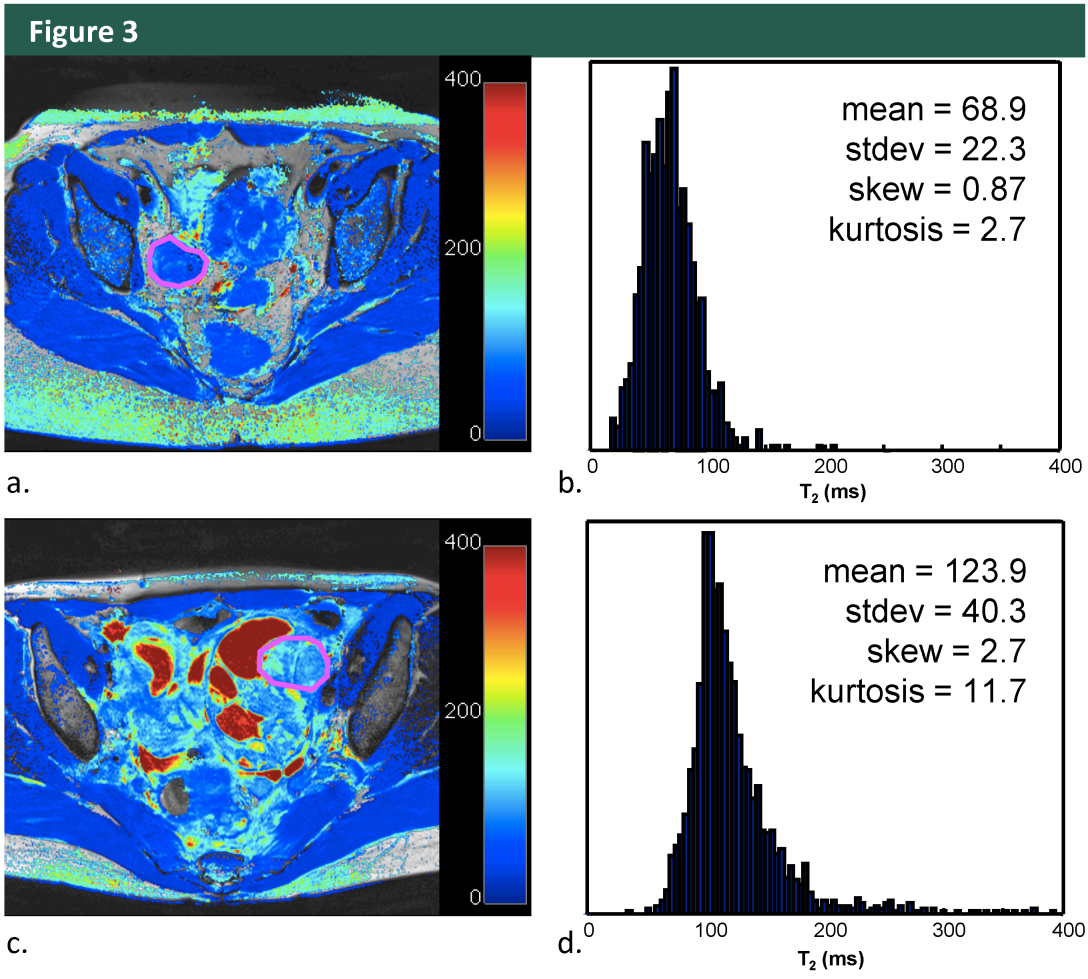

Table 6. AUC for T_2 imaging weighted imaging in solid ROIs.

Parameter	Benign		Malignant		AUC of Mean Only		Cross-Validation Adjusted AUC of Combined Values*	
	N subjec	N RO	N subjec	N RO	AUC	95% CI	AUC	95% CI
T_2 w	7	8	11	19	0.83	(0.64, 0.99)	0.68	(0.45, 1)
T_2 w-ref	7	8	11	19	0.85	(0.67, 0.97)	0.78	(0.63, 1)
T_2 map	7	7	10	18	0.81	(0.56, 1)	0.90	(0.83, 1)

*A linear model of the mean, standard deviation, skewness and kurtosis

References

1. American, Cancer Society. Cancer Facts and Figures 2009. Atlanta: American Cancer Society, 2009.
2. Munkarah A, Chatterjee M, Tainsky M. Update on ovarian cancer screening. Curr Opin Obstet Gynecol 2007;19:22-26.
3. Earle CC, Schrag D, Neville BA, et al. Effect of surgeon specialty on processes of care and outcomes for ovarian cancer patients. J Natl Cancer Inst 2006;98(3):172-180.
4. Mercado C, Zingmond D, Karlan BY, et al. Quality of care in advanced ovarian cancer: the importance of provider specialty. Gynecol Oncol 2010;117(1):18-22.
5. Menon U, Gentry-Maharaj A, Hallett R, et al. Sensitivity and specificity of multimodal and ultrasound screening for ovarian cancer, and stage distribution of detected cancers: results of the prevalence screen of the UK Collaborative Trial of Ovarian Cancer Screening (UKCTOCS). Lancet Oncol 2009;10(4): 327-340.
6. Buy JN, Ghossain MA, Hugol D, et al. Characterization of adnexal masses: combination of color Doppler and conventional sonography compared with spectral Doppler analysis alone and conventional sonography alone. AJR 1996;166:385-393.
7. Stein SM, Laifer-Narin S, Johnson MB, et al. Differentiation of benign and malignant adnexal masses: relative value of gray-scale, color Doppler, and spectral Doppler sonography. AJR 1995;164(2):381-386.
8. Levine D, Feldstein VA, Babcock CJ, Filly RA. Sonography of ovarian masses: poor sensitivity of resistive index for identiying malignant lesions. AJR 1994;162:1355-1359.
9. Rehn M, Lohmann K, Rempen A. Transvaginal ultrasonography of pelvic masses: evaluation of B-mode technique and Doppler ultrasonography. Am J Obstet Gynecol 1996;175(1):97-104.
10. Buys SS, Partridge E, Greene MH, et al. PLCO Project Team. Ovarian cancer screening in the Prostate, Lung, Colorectal and Ovarian (PLCO) cancer screening trial; findings from the intial screen of a randomized trial. Am J Obstet Gynecol 2005;193(5):1630-1639.
11. Buys SS, Partridge E, Black A, et al. for the PLCO Project Team. Effect of screening on ovarian cancer mortality: the prostate, lung, colorectal and ovarian (PLCO) cancer screening randomized controlled trial. JAMA 2011;305(22):2295-2303.
12. van Nagell JR, DePriest PD, Ueland FR, et al. Ovarian cancer screening with annual transvaginal sonography: findings of 25,000 women screened. Cancer 2007;109(9):1887-1896.
13. Booth SJ, Turnbull LW, Poole DR, Richmond I. The accurate staging of cancer using 3T magnetic resonance imaging – a realistic option. BJOG 2008;115:894-901.
14. Hricak H, Chen M, Coakley FV, et al. Complex adnexal masses: detection and characterization with MR imaging - multivariate analysis. Radiology 2000;214:39-46.
15. Sohaib SA, Sahdev A, Van Trappen P, Jacobs IJ, Reznek RH. Characterization of adnexal mass lesions on MR imaging. Am J Roentgenol. 2003, Vols. 180(5):1297-1304.

16. Thomassin-Naggara I, Toussaint I, Perrot N, et al. Characterization of complex adnexal masses: value of adding perfusion- and diffusion-weighted MR imaging to conventional MR imaging. Radiology 2011;258(3):793-803.
17. Thomassin-Naggara I, Darai E, Cuenod CA, Rouzier R, Callard P, Bazot M. Dynamic contrast-enhanced magnetic resonance imaging: a useful tool for charcterizing ovarian epithelial tumors. J Magn Reson Imaging 2008;28:111-120.
18. Thomassin-Naggara I, Bazot M, Daraï E, Callard P, Thomassin J, Cuenod CA. Epithelial ovarian tumors: value of dynamic contrast-enhanced MR imaging and correlation with tumor angiogenesis. Radiology 2008;248(1):148-159.
19. Moteki T, Ishizaka H. Diffusion-weighted EPI of cystic ovarian lesions: evaluation of cystic contents using apparent diffusion coefficients. J Magn Reson Imaging 2000;12(6):1014-1019.
20. Thomassin-Naggara I, Darai E, Cuenod CA, et al. Contribution of diffusion-weighted MR imaging for predicting benignity of complex adnexal masses. Eur Radiol 2009;19:1544-1552.
21. Le Bihan D, Breton E, Lallemand D, Aubin ML, Vignaud J, Laval-Jeantet M. Separation of diffusion and perfusion in intravoxel incoherent motion MR imaging. Radiology 1998;168(2):497-505.
22. Guo JY, Reddick WE, Rosen MA, Song HK. Dynamic contrast-enhanced magnetic resonance imaging parameters independent of baseline T10 values. Magn Reson Imaging 2009;27(9):1208-1215.
23. Parker GJ, Roberts C, Macdonald A, et al. Experimentally-derived functional form for a population-averaged high-temporal-resolution arterial input function for dynamic contrast-enhanced MRI. Magn Reson Med 2006;56(5):993-1000.
24. Tofts PS, Brix G, Buckley DL, et al. Estimating kinetic parameters from dynamic contrast-enhanced T1-weighted MRI of a diffusable tracer: standardized quantities and symbols. J Magn Reson Imaging 1999;10:223-232.
25. OsiriX Imaging Software: Advanced Open-Source PACS Workstation DICOM Viewer. OsiriX Website. http://www.osirix-viewer.com. Accessed March 30, 2012.
26. Diggle PJ, Heagerty P, Liang KY, Zeger SL. Analysis of Longitudinal Data, 2nd Edition. Oxford University Press, New York, NY, 2002.
27. Hastie T, Tibshirani R, Friedman J. The Elements of Statistical Learning: Data Mining, Inference and Prediction, Springer, New York, NY, 2001.
28. Efron B, Tibshirani RJ. An Introduction to the Bootstrap, CRC Press, Boca Raton, FL, 1998.
29. R Project. R Version 2.14.2012-03-14. R Project Website. http://cran.r-project.org/doc/FAQ/R-FAQ.html. ISBN 3-900051-08-9. Accessed March 30, 2012.
30. Katayama M, Masui T, Kobayashi S, et al. DIffusion-weighted echo planar imaging of ovarian tumors: is it useful to measure apparent diffusion coeffecients? J Comp Assist Tomogr 2002;26(2):250-256.
31. Kyriazi S, Collins DJ, Messiou C, et al. Metastatic ovarian and peritoneal cancer: assessing chemotherapy response with diffusion-weighted MR imaging- value of histogram analysis of apparent diffusion coefficients. Radiology 2011;261(1):182-192.

32. Nakayama T, Yoshimitsu K, Irie H, et al. Diffusion-weighted echo-planar MR imaging and ADC mapping in the differential diagnosis of ovarian cystic masses: usefulness of detecting keratinoid substances in mature cystic teratomas. J Magn Reson Imaging 2005;22:271-278.
33. Namimoto T, Awai K, Nakaura T, Yanaga Y, Hirai T, Yamashita Y. Role of diffusion-weighted imaging in the diagnosis of gynecological diseases. Eur Radiol 2009;19:745-760.